NANO LETTERS

pubs.acs.org/NanoLett

Dependence of Carrier Mobility on Nanocrystal Size and Ligand Length in PbSe Nanocrystal Solids

Yao Liu,[†] Markelle Gibbs,[†] James Puthussery,[†] Steven Gaik,[‡] Rachelle Ihly,[†] Hugh W. Hillhouse,[‡] and Matt Law*[,†]

[†]Department of Chemistry, University of California, Irvine, Irvine, California 92697 and [‡]School of Chemical Engineering, Purdue University, West Lafayette, Indiana 47907

ABSTRACT We measure the room-temperature electron and hole field-effect mobilities (μ_{FE}) of a series of alkanedithiol-treated PbSe nanocrystal (NC) films as a function of NC size and the length of the alkane chain. We find that carrier mobilities decrease exponentially with increasing ligand length according to the scaling parameter $\beta = 1.08-1.10$ Å^{-1}, as expected for hopping transport in granular conductors with alkane tunnel barriers. An electronic coupling energy as large as 8 meV is calculated from the mobility data. Mobilities increase by 1−2 orders of magnitude with increasing NC diameter (up to 0.07 and 0.03 cm^2 V^{-1} s^{-1} for electrons and holes, respectively); the electron mobility peaks at a NC size of ∼6 nm and then decreases for larger NCs, whereas the hole mobility shows a monotonic increase. The size-mobility trends seem to be driven primarily by the smaller number of hops required for transport through arrays of larger NCs but may also reflect a systematic decrease in the depth of trap states with decreasing NC band gap. We find that carrier mobility is independent of the polydispersity of the NC samples, which can be understood if percolation networks of the larger-diameter, smaller-band-gap NCs carry most of the current in these NC solids. Our results establish a baseline for mobility trends in PbSe NC solids, with implications for fabricating high-mobility NC-based optoelectronic devices.

KEYWORDS PbSe, nanocrystal, quantum dot, mobility, field-effect transistor

Three-dimensional films of colloidal semiconductor nanocrystals (NC solids) are a new class of granular electronic material with potential applications in electronic and optoelectronic devices, including field-effect transistors,[1,2] photodetectors,[3] and solar cells.[4−7] The electronic properties of colloidal NC solids can in principle be controlled by adjusting NC composition, size, shape, monodispersity, capping ligand, and surface chemistry as well as the degree of superlattice order in the films. The strength of quantum mechanical electronic coupling between NCs (i.e., the coupling energy $h\Gamma$, where Γ is the rate of carrier hopping between two NCs and h is Planck's constant) depends in large part on the inter-NC distance (the tunnel barrier width)[2,8−10] and the nature of the inter-NC barrier material (the tunnel barrier height). Exchanging long-chain organic ligands with short ones improves electronic coupling by decreasing the barrier width, thereby increasing Γ. Similarly, for a given NC spacing, replacing saturated ligands with either conjugated ligands or an inorganic material of smaller effective band gap (or lower effective mass) should increase coupling and the hopping rate by reducing the effective height of the barrier. Strong electronic coupling promotes high carrier mobility and conductivity, which are desirable properties for many optoelectronic devices.

Near room temperature, charge transport in lead chalcogenide (PbX, X = S, Se, Te) NC solids may be further limited by disorder. PbX NC solids tend to be disordered materials because (i) chemically synthesized NCs inevitably have a distribution of sizes/shapes and thus energy levels, (ii) the inter-NC distance is locally non-uniform (imperfect short-range order), and (iii) the superlattice order of conductive NC films is often fairly poor (imperfect long-range order). Disorder may have major deleterious effects on carrier mobility: positional and orientational disorder disrupts the formation of extended Bloch-like wave functions (mini-bands), while energetic disorder (the size-dependent spread in NC site energies) results in thermally activated transport, further limiting the mobility. Minimizing these forms of disorder is important for improving electronic transport in PbX NC films.

A major goal of current research on NC solids is to devise practical methods for creating well-coupled, geometrically ordered, and robust PbX NC films with the high carrier mobilities (>50 cm^2 V^{-1} s^{-1}) and long carrier lifetimes and diffusion lengths needed for next-generation optoelectronic devices such as solar cells. Rationally achieving this goal requires a deep understanding of charge transport in NC materials. Here we describe how the carrier mobility depends on ligand length and NC size in alkanedithiol-coated PbSe NC field-effect transistors (FETs). Room-temperature measurements show that electron and hole mobilities increase exponentially with decreasing ligand length, demon-

* Address correspondence to matt.law@uci.edu.
Received for review: 04/12/2010
Published on Web: 04/21/2010

DOI: 10.1021/nl101284k | *Nano Lett.* **2010,** *10,* 1960–1969

strating the inverse relationship between coupling energy and inter-NC distance. Meanwhile, FET measurements as a function of NC size show that, at a constant ligand length, mobilities depend strongly on the average NC size but are essentially independent of the size distribution (i.e., the energy disorder). The weak influence of NC polydispersity on mobility can be understood if the NC films are heterogeneous on the nanoscale such that charge carriers can avoid large activation energies by traveling through percolation networks of the bigger NCs in a film. These trends with ligand length and NC size suggest that electron and hole mobilities of $\sim$1 $cm^2\ V^{-1}\ s^{-1}$ can be obtained using glassy, thiol-treated PbSe NC films that employ the shortest possible ligands (e.g., methanethiol). However, improving NC monodispersity is unlikely to enhance mobilities as long as the NC films have poor translational order that prevents coherent tunneling via extended states.

Experimental Section. ***Materials.*** Lead oxide (PbO, 99.999%), selenium (99.99%), oleic acid (OA, tech. grade, 90%), diphenylphosphine (DPP, 98%), 1-octadecene (ODE, 90%), 1,3-propanedithiol (PDT, >98%), 1,4-butanedithiol (BuDT, >98%), and anhydrous solvents were purchased from Aldrich and used as received. Trioctylphosphine (TOP, tech. grade, >90%) and 1,2-ethanedithiol (EDT, >98%) were acquired from Fluka. 1,5-Pentanedithiol (PenDT, >98%) and 1,6-hexanedithiol (HDT, >98%) were purchased from Acros and Alfa Aesar, respectively.

NC Synthesis. The NCs were synthesized and purified using standard air-free techniques. In a typical synthesis, 1.09 g of PbO (4.9 mmol), 3.45 g of OA (12.2 mmol), and 13.25 g of ODE were degassed in a three-neck flask for 10 min at room temperature and 10 min at 100 °C and then heated at 180 °C for at least 1 h under flowing nitrogen to dissolve the PbO and dry the solution. Next, 15 mL of a 1 M TOP-Se solution (15 mmol) containing 0.13 mL DPP was rapidly injected into the hot lead oleate solution. PbSe NC nucleation was instantaneous. Once the desired growth time had elapsed (1−20 min), the reaction was quenched with a water bath and injection of 15 mL of dry hexane. The NCs were purified by precipitation three times in hexane/ethanol and stored in a glovebox.

Fabrication of NC Films. A mechanical dip coater mounted inside of a glovebox (DC Multi-4, Nima Technology) was used to prepare PbSe NC films via a layer-by-layer procedure described in detail elsewhere.[11,12] Briefly, the substrates (prepatterned FET substrates, glass slides, or double-side-polished *i*-Si(100) wafers, cleaned by sonication in acetone followed by rinses in acetone and hexane and drying under an N_2 flow) were alternately dipped into a 2 mg mL^{-1} solution of NCs in dry hexane and then a 1 mM solution of alkanedithiol in dry acetonitrile. In the case of the butanedithiol, pentanedithiol, and hexanedithiol treatments (the nonvolatile dithiols), a third beaker containing pure acetonitrile was used to rinse the films after each dip in the dithiol solution in order to remove any dithiol residue. We fabricated films with thicknesses in the range of 20−250 nm (thin for FETs and thick for UV−vis and FTIR studies).

Characterization. Transmission electron microscopy (TEM) characterization was performed on a Philips CM 20 operating at 200 kV. The particle size and size distribution were calculated based on measurements of at least 100 NCs. A Zeiss Ultra 55 Plus field emission scanning electron microscope (SEM) was used to image the NC films. Optical absorption data were acquired with a PerkinElmer Lambda 950 spectrophotometer equipped with an integrating sphere. Fourier transform infrared (FTIR) data were taken on 200 nm thick films using a Jasco 4100 FTIR spectrometer.

Field-Effect Transistor Measurements. NC films were dip cast onto degenerately doped silicon substrates that were coated with a 200 nm thick thermal SiO_2 gate oxide and patterned with source/drain electrodes (5 nm Ti/35 nm Au, 10 or 25 μm channel length, 1000 μm width). Film thicknesses of 20−35 nm (3−6 NCs thick) were used. Unwanted areas of each film were removed with a swab. FET measurements were performed in a glovebox with a homemade probe station using a Keithley 2636A dual-channel SourceMeter driven by LabVIEW software. Consistent with previous results,[11,13] we found the source−drain currents of these FETs to be time dependent (quasi-exponential decay) upon a change in gate voltage. I_D-V_{SD} and I_D-V_G curves were therefore acquired quickly (0.4−0.8 s) to minimize the distorting effects of the slow transient process(es) on the output and transfer characteristics of the devices (see text). Electron and hole mobilities μ were calculated from transfer curves acquired at positive and negative V_{SD}, respectively, according to the gradual channel approximation equation in the linear regime

$$\left.\frac{\partial I_D}{\partial V_G}\right|_{V_{SD}=\text{constant}} = \frac{WC_{OX}V_{SD}}{L}\mu_{lin}$$

where W is the channel width, L the channel length, and C_{ox} the capacitance per unit area of the gate oxide. The carrier mobilities reported here are averages of at least six devices.

Results and Discussion. ***NC Characterization.*** Figure 1 presents transmission electron microscopy (TEM) images of six of the PbSe NC samples used in this study. The smallest NCs (3.1 nm diameter) are a mixture of spheroids and tetrahedra, while the largest NCs (8.6 nm diameter) are cubes mixed with some cubic dimers. All samples show fairly tight diameter distributions ($\sigma = 5-11\%$), corresponding to a diameter spread of about one unit cell (except for the largest NCs, where 2σ is about two unit cells). The first excitonic absorption energy of the six samples varies from 0.56 to 1.2 eV, in good agreement with previously reported diameter−band gap curves for PbSe NCs (see Figures S1 and S2 in the Supporting Information).

FET Properties. Our alkanedithiol-treated PbSe NC solids act as thin film transistors with ambipolar conductivity

DOI: 10.1021/nl101284k | *Nano Lett.* **2010,** *10,* 1960−1969

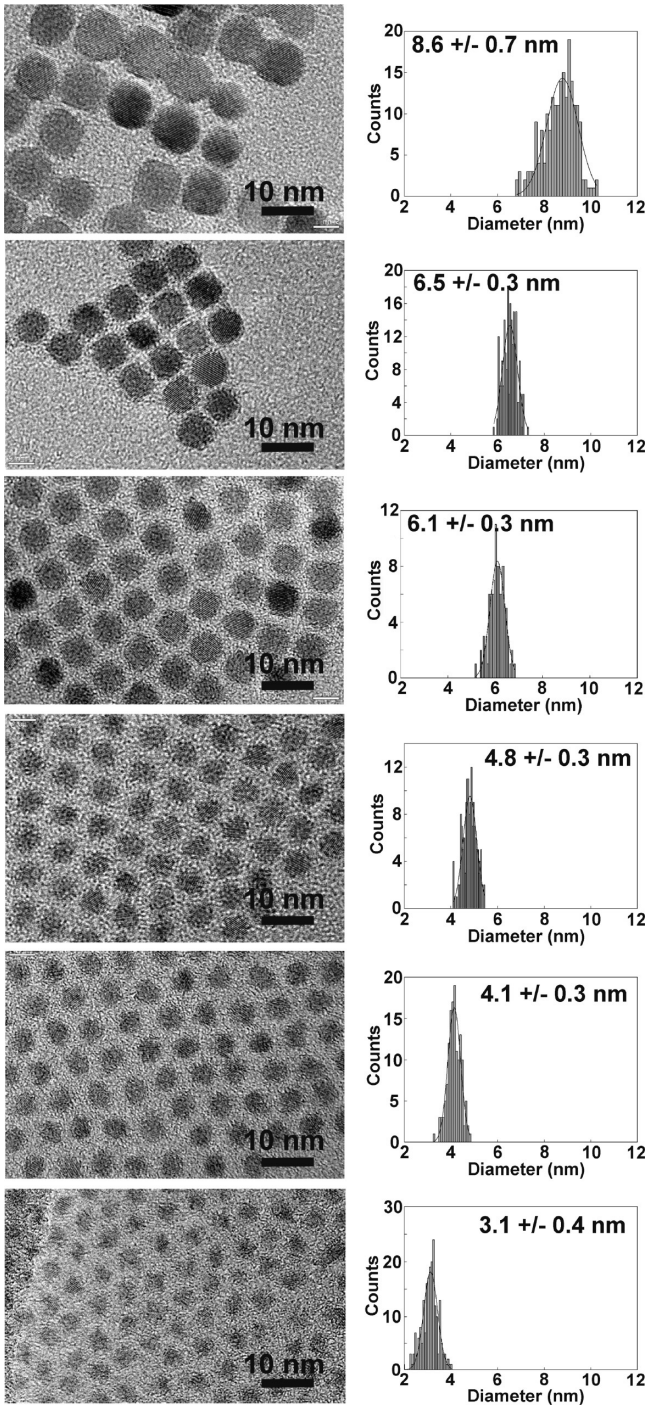

FIGURE 1. TEM images and sizing histograms of six of the batches of oleate-capped PbSe NCs used in this study.

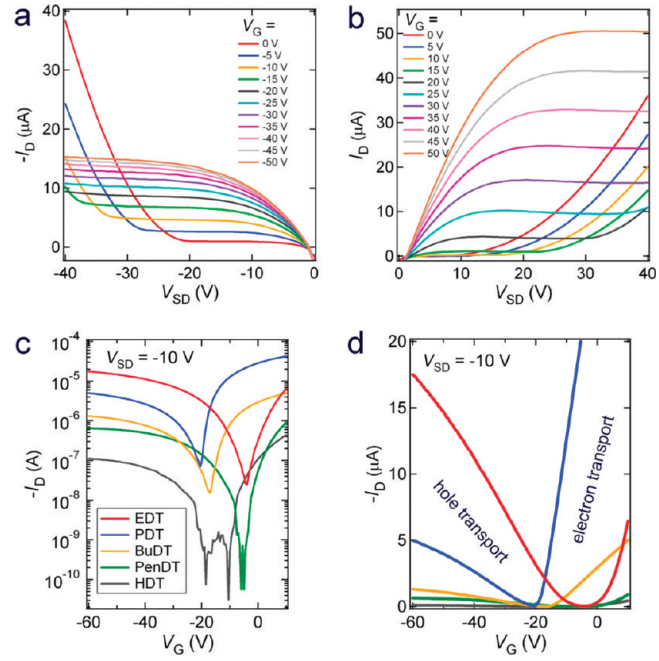

FIGURE 2. Output characteristics of a typical ambipolar PbSe NC FET (fabricated from 6.1 nm diameter NCs treated in 1,2-ethanedithiol) at (a) negative V_{SD} and (b) positive V_{SD}. (c) Transfer characteristics of a series of alkanedithiol-treated devices on logarithmic and (d) linear scales at $V_{SD} = -10$ V. Color coding is the same for both graphs. The asymmetric V-shape of each I_D-V_G plot indicates unequal electron and hole mobilities. EDT, PDT, BuDT, PenDT, and HDT are 1,2-ethanedithiol, 1,3-propanedithiol, 1,4-butanedithiol, 1,5-pentanedithiol, and 1,6-hexanedithiol, respectively. NC diameter = 6.1 nm. Channel dimensions: length = 10 μm; width = 1000 μm; film thickness = 20−35 nm.

(Figure 2). For instance, the device in parts a and b of Figure 2 switches from hole (p channel) to electron (n channel) conduction as the gate voltage (V_G) is swept from 0 to ±50 V. The electron mobility calculated from the drain current (I_D)−V_G characteristics in the linear region of source−drain bias (V_{SD}) (Figure 2c,d) was consistently 2−6 times larger than the hole mobility of the same device, with values as high as 0.07 and 0.03 cm^2 V^{-1} s^{-1}, respectively. The larger mobility of electrons in PbSe NC films has been observed previously[2,11,14] and attributed to either a smaller barrier height for inter-NC electron transport[15] or a larger density of states within the band gap induced by the chemical treatment used to electronically couple the NC films.[14] Our results support the latter explanation (see below).

These alkanedithiol-treated NC FETs suffer from transient drain currents[11] that can distort the shapes of output and transfer plots and lead to incorrect mobility values unless the measurements are carried out quickly compared to the characteristic time of the transients. Figure 3a shows a typical I_D transient. Here, stepping the gate voltage from 0 to −10 V causes a sudden change in I_D, as expected, but this is followed by an exponential relaxation of I_D toward its value at $V_G = 0$ V. This transient behavior is consistent with a slow screening of the applied gate field by carriers trapped at the oxide surface or on the first layer of NCs, as discussed elsewhere,[11] or by some more complicated mechanism. Output curves acquired slowly will be a superposition of the "true" curve shape and an exponential decay. Depending on the ratio of the measurement time to the time constant of the I_D transient, the drain current of a given device may (i) saturate, (ii) peak, or (iii) peak and then increase linearly with V_{SD}. The curve shape is selectable by changing the V_{SD} sweep rate (Figure 3b). Note also that slow transients can

DOI: 10.1021/nl101284k | *Nano Lett.* **2010,** *10,* 1960–1969

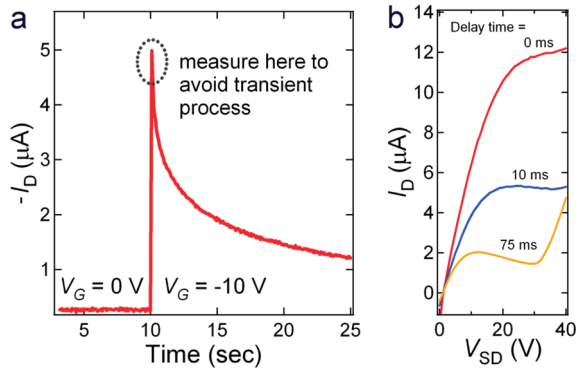

FIGURE 3. (a) Time trace of I_D for a typical PbSe NC FET, showing a quasi-exponential decay after a change in V_G. $V_{SD} = -10$ V. Measurements should be made quickly to avoid significant distortion of the output and transfer data. (b) Output curves of an EDT-treated device at three different V_{SD} sweep rates, scanning from 0 to 40 V. Very slow measurements sample the entire exponential transient and result in a peak at low V_{SD} followed by a linear increase in I_D with V_{SD}.

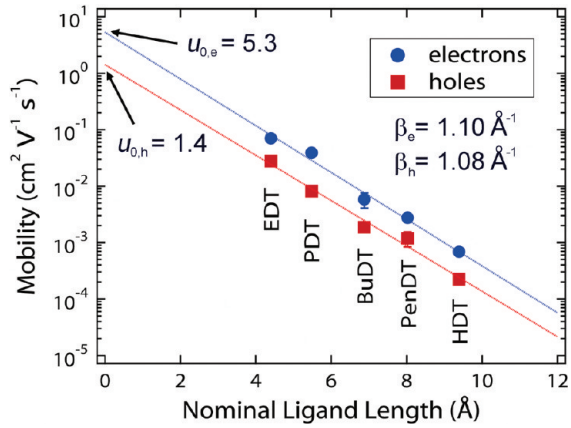

FIGURE 4. Carrier mobility as a function of ligand length in ambipolar PbSe NC field-effect transistors (6.1 nm NCs). Each data point is the average of 6−12 devices prepared on different days. Error bars are mostly smaller than the symbols. Molecular lengths were calculated using MM2 energy minimization in the ChemBio 3D software package considering only the projected sulfur-to-sulfur distance (~1.5 Å per C−S bond and ~1.25 Å per C−C bond)[19] and neglecting S−Pb bonding. The plot assumes that the inter-NC spacing is proportional to the extended length of each ligand (see text). Channel dimensions: length =10 μm; width =1000 μm; film thickness =20−35 nm.

transform linear I_D-V_{SD} plots into curves that seem to possess the linear and saturation regions of an ideal FET, potentially leading to incorrect mobility values. Since we have not found a way to stop the transients of the alkanedithiol-treated devices, we simply measure the output and transfer data as quickly as possible (<500 ms) in order to sample only a small part of the transient (approximately the dotted oval in Figure 3a) and thereby minimize the distortion. This procedure produces transfer curves that are free from hysteresis. We emphasize that the mobilities calculated from our data are probably lower bounds because our apparatus cannot detect transients that are faster than ~10 ms, if such transients exist.

Mobility Dependence on Ligand Length. At room temperature, long-range charge transport in our PbSe NC solids occurs by nearest-neighbor hopping, i.e., a series of incoherent tunneling transitions between adjacent NCs. Thousands of individual hops are required for a carrier to traverse the 10 μm FET channel. The NCs form an array of localized but coupled electronic sites with significant positional disorder and a Gaussian spread of site energies (as inferred from the Gaussian line shape of excitonic features in optical absorption spectra). The tunneling transition rate Γ_{ij} of a charge carrier hopping from a NC of energy E_i to one of energy E_j across a tunnel barrier of width d can be described by a Miller−Abrahams expression,[16] which is a product of exponential distance and energy terms

$$\Gamma_{ij} = \Gamma_0 \exp(-\beta d)\begin{cases} \exp\left[-\dfrac{E_j - E_i}{kT}\right] & (E_j > E_i) \\ 1 & (E_j \le E_i) \end{cases} \quad (1)$$

Here, Γ_0 is an attempt frequency, β is the tunneling decay constant, and T is the temperature. The Boltzmann term is included because hopping to a state of higher energy is an activated process. The NC energies include both the site energies and the charging (Coulomb) energies. At large applied fields, β and $(E_j - E_i)$ can be modified by the additional field-induced potential difference between the NCs. Therefore, V_{SD} was chosen such that the field across individual tunnel barriers was smaller than kT (specifically, <4 mV/nm) in order to minimize field-induced effects on the barrier height and the carrier mobility.

Equation 1 provides a basis for calculating the mobility of charge carriers in disordered colloidal NC solids at any temperature. The mobility in the nearest-neighbor hopping regime (where the thermal energy is comparable to or larger than the NC energy spread ΔE) is given by[17]

$$\mu = \mu_0 \exp(-0.865\beta\tilde{d}) \exp\left[-\frac{\Delta E}{kT}\right] \quad (2)$$

Equation 2 predicts an exponential decrease in mobility with increasing average barrier width $\tilde{d}$ for a given NC sample at fixed temperature. Figure 4 presents the average electron and hole mobilities in the linear regime (μ_{lin}) for ambipolar FETs fabricated from 6.1 nm diameter PbSe NCs treated with one of a series of alkanedithiol ligands $(HS(CH_2)_nSH$, with $n = 2-6$). A single batch of NCs was used so that the site energy distribution and charging energy of the NC films were held constant. The data are linear on a semilog plot, with the highest electron and hole mobilities (0.07 and 0.03 cm^2 V^{-1} s^{-1}, respectively) measured with the shortest molecule (EDT) and the lowest mobilities (7×10^{-4} and 2×10^{-4} cm^2 V^{-1} s^{-1}) measured with the longest molecule (HDT).

DOI: 10.1021/nl101284k | *Nano Lett.* **2010,** *10,* 1960–1969

Linear fits to the data yield tunneling decay constants β of 1.10 and 1.08 Å^{-1} for electron and hole transport. These values are consistent with tunneling conductance measurements across alkanethiol and dithiol self-assembled monolayers (SAMs)[18−23] and metal NC arrays.[24,25] In the WKB approximation, $\beta = (2m^*\bar{E}_{barrier}/\hbar^2)^{1/2}$, where $\bar{E}_{barrier}$ is the average barrier height. Using $m^* = 0.28m_e$ for the effective carrier mass in the aliphatic ligand layer,[26] we calculate a barrier height for electron transport of ∼1.6 eV, in agreement with many SAM studies.[24] The nearly identical β_e and β_h values suggest a similar barrier height for holes and thus an effective HOMO−LUMO gap for the bound alkanedithiol linkers of approximately 3.2 eV + $E_g \approx$ 3.9 eV, where E_g is the excitonic gap of the NCs in the FETs. The fact that this value is significantly smaller than the HOMO−LUMO gap for alkane chains (∼8−10 eV) might be explained by hybridization of molecular and NC orbitals that introduces a significant density of states in the molecular junction and thereby lowers the effective barrier to transport to ∼1−2 eV.[27,20] The similar β_e and β_h values are also evidence that the larger mobility for electrons arises from a larger electron density of states (resulting in a larger μ_0) rather than different hopping barrier heights for electrons and holes.[14,15]

The question arises as to whether the hopping barrier width is in fact set by the length of the alkanedithiol ligands used to prepare the films. We attempted to measure the inter-NC spacing of a series of films using grazing incidence small-angle X-ray scattering (GISAXS), but the results, presented in Figure S3, were largely inconclusive for several reasons. First, the alkanedithiolate ligands are unstable in air; even the brief air exposure required to transfer the films into the GISAXS chamber triggers oxidative desorption and configurational changes of the dithiolates,[11] altering the NC spacing by a varying but unknown amount. Second, the average electron density of the films increased slowly during the GISAXS experiments (determined from the measured increase in the critical angle). This indicates that the X-ray photons (or extended exposure to vacuum) assist ligand desorption. These two effects led to an error of at least ±2 Å in the measured NC spacing. This error is comparable to the anticipated difference in NC spacing between EDT- and HDT-treated films (∼5 Å) and so obscures any bona fide trends in the data. Thus, while the approximate magnitude of the inter-NC spacing determined by GISAXS is reasonable, the trend in inter-NC spacing as a function of dithiol treatment (Figure S3) is not a good measure of the true relative spacings for the pristine NC films of Figure 4.

Although we are unable to provide a convincing measurement of the inter-NC distance for the dithiol-treated NC films, several indirect lines of evidence support the notion that it is determined by the length of the dithiol ligands. FTIR spectra show that all five alkanedithiol treatments completely remove the original oleate capping and result in a significant amount of dithiolate adsorption within the films (Figure S4), with progressively larger integrated C−H stretch intensities for longer dithiols at constant film thickness. The FTIR results suggest that dithiols are the only ligands present in the NC films in appreciable concentration. This result, combined with the unambiguous mobility trends and reasonable β values of Figure 4, provides a strong basis for inferring that the inter-NC distance is set by the projected alkanedithiol length and that the barrier width increases by ∼1.25 Å for each additional methylene group in the alkane chain. Note that while the slopes of the fits (β) are physically reasonable, their intercepts (μ_0) may be underestimated because we neglect the Pb−S bond distance when calculating the ligand lengths.

We can use the Einstein−Smoluchowski equation, $\mu = (e/2kT)\Delta^2\Gamma$, where Δ is the tunneling distance, to determine the coupling energy $h\Gamma$ between neighboring NCs in the films. For electrons in the EDT-treated devices, we find $\Gamma = 2 \times 10^{12}$ s^{-1}, corresponding to a coupling energy of 8 meV. The values are $\Gamma = 4 \times 10^9$ s^{-1} and $h\Gamma = 16$ μeV for HDT-treated devices. An electronic coupling of 8 meV should produce a comparable red shift of the first excitonic absorption, and EDT-treated films indeed show a ∼10 meV red shift relative to HDT-treated films (Figure 5a). In turn, the HDT-treated films are red-shifted by 22 meV relative to untreated films (which still possess their original oleate capping ligands). Since the coupling energy of the HDT-treated films is very small (of order 10 μeV), we conclude that the large red shift observed with HDT-treated films is due entirely to non-$h\Gamma$ effects, such as the increased average dielectric constant of the film upon replacing oleate with HDT and/or the relaxation of quantum confinement upon replacement of an "oxide-like" carboxylate ligand layer with a "sulfide-like" thiol layer.[28]

By comparing the coupling energy and optical band gap of these films, it is possible to quantify the contribution of electronic coupling to the overall excitonic red shift (Figure 5b). We find that coupling becomes an appreciable and increasingly large fraction of the red shift as the ligand length decreases below 6−8 Å. Extrapolating the plots to zero barrier width suggests that the use of organic ligands shorter than EDT could boost the coupling energy and electron mobility to >250 meV and >1 cm^2 V^{-1} s^{-1}. Further improvements in mobility might be achieved by replacing the organic spacer with an inorganic material featuring a smaller barrier height and lower effective mass to reduce the value of β.[29] Greatly improving the superlattice order of the films could also increase the carrier mobility (see below).

We are aware of two previous studies of the coupling energy in PbSe NC solids, both of which cite larger values for $h\Gamma$ than found here. Liljeroth et al. reported strong microscopic variations in coupling energy for 2D arrays of thermally annealed PbSe NCs by scanning tunneling spectroscopy (STS).[15] On the basis of level broadening in STS spectra, they concluded that individual NCs are predominantly coupled in a band-selective fashion, with a typical coupling strength of 50−150 meV between the electron

DOI: 10.1021/nl101284k | Nano Lett. 2010, 10, 1960−1969

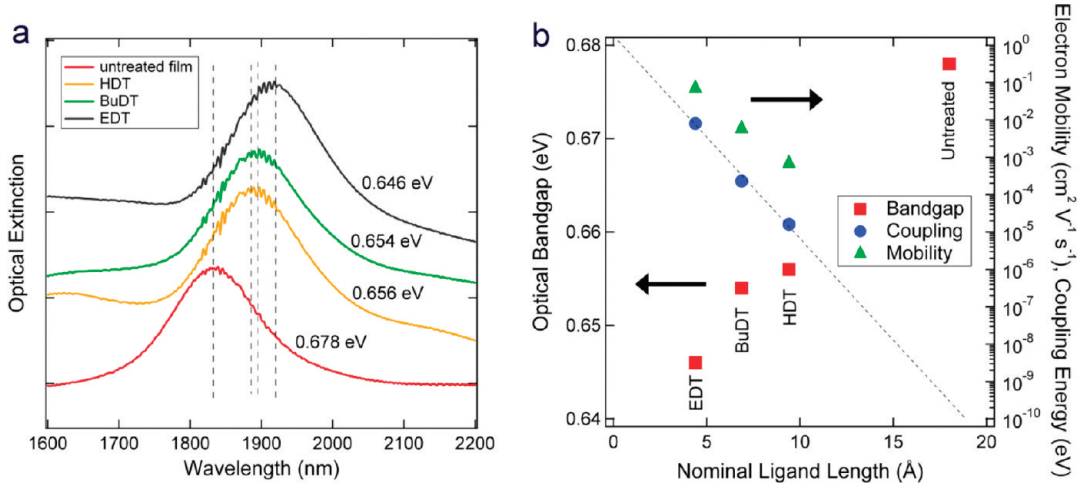

FIGURE 5. (a) Position of the first excitonic absorption peak of PbSe NC films on glass substrates as a function of chemical treatment (6.1 nm diameter NCs). (b) Coupling energy, electron mobility and optical band gap of these films. The large red shift of HDT-treated films relative to untreated films is caused by factors other than electronic coupling, while the red shift of EDT-treated films relative to HDT-treated films is dominated by such coupling. The dotted line extrapolates the coupling energy to narrow and wide hopping barriers.

levels. Other NCs in the same films showed band gap narrowing of ~450 meV and very strong coupling for both electron and hole states. However, our own optical absorption measurements of 3D films of 5.7 nm PbSe NCs prepared according to Liljeroth's procedure show an absorption red shift of only 9 meV (less than the HDT-treated films) implying a small degree of coupling between NCs. We believe that the discrepancy is a result of the different spatial scales of STS and FET/UV−vis measurements: as a local probe, STS can detect small domains of tightly coupled NCs to which our long-range transport measurements and ensemble optical measurements are insensitive. In the second report, Williams et al. used red shifts in ATR-FTIR spectra to estimate the coupling energy in 2D partial monolayers of hydrazine-treated NCs.[30] They found large red shifts of ~80 and ~150 meV for 6 and 4 nm NCs and, by attributing the entire red shift to electronic coupling, arrived at coupling energies of 7 and 13 meV, respectively. These authors also reported that red shifts were 3−4 times larger for 2D films compared to 3D films with the same chemical treatment, citing the less significant geometric frustration in 2D than in 3D assemblies as responsible for this "extra" red shift. Motivated by the work of Williams, we carefully measured the absorbance red shift in 2D submonolayers of EDT-treated NCs but found no difference between 2D and 3D films (see Figure S5 in Supporting Information). These results show that red shifts and coupling energies are not necessarily larger in 2D NC assemblies; clearly, nongeometric factors also play a role in determining the magnitude of excitonic red shifts in NC films.

Mobility Dependence on NC Size. In Figure 6, we plot the field-effect mobilities (μ_{lin}) of a series of EDT-treated PbSe NC FETs made from NC samples of different average size (diameter = 3.1−8.6 nm) and different size polydispersity. Electron and hole mobilities are observed to increase by 1−2 orders of magnitude with increasing NC size (Figure 6a−c); the electron mobility peaks at a NC diameter of ~6 nm and then declines for larger NCs, whereas the hole mobility shows a monotonic increase. Unlike the dependence of mobility on ligand length, which is dominated by a single factor (the exponential tunneling rate), the mobility trends with NC size may convolve several factors, including (i) the size-dependent NC charging energy E_C, which is the energy required to add a charge to a neutral NC in a film, (ii) differences in the site energy disorder $\Delta\alpha$ (polydispersity) of the various NC samples, (iii) the smaller number of hops needed for carriers to travel across FET channels composed of larger NCs, and (iv) changes in the depth of trap states with NC band gap. Changing the NC size may also change the shape, faceting, surface charge distribution, surface trap density, carrier confinement, and packing density/geometry of NCs within the films, all of which can affect the mobility in nontrivial ways. Therefore, we expect a quantitative understanding of the dependence of mobility on NC size to be challenging to obtain.

We first show that the mobility−size relationships in Figure 6 cannot be explained by the size-dependent NC charging energy. The charging energy of a semiconductor NC within a NC solid is estimated as $E_c = e^2/[2(C_S + 9C_M)]$,[31] where C_S is the self-capacitance and C_M the mutual capacitance of adjacent NCs. Here we assume an average of nine nearest neighbors for NCs in the FET channel. In the case of a dielectric sphere of size-dependent dielectric constant $\varepsilon_{in}(r)$ embedded in a material of much smaller average dielectric constant ε_{out}, we have[32]

$$C_S^{-1} \approx \frac{1}{4\pi\varepsilon_0 r}\left(\frac{\varepsilon_{in}(r) - \varepsilon_{out}}{\varepsilon_{in}(r)\varepsilon_{out}}\right) + \frac{0.94}{4\pi\varepsilon_0\varepsilon_{in}(r)r}\left(\frac{\varepsilon_{in}(r) - \varepsilon_{out}}{\varepsilon_{in}(r) + \varepsilon_{out}}\right) \quad (2a)$$

and

DOI: 10.1021/nl101284k | *Nano Lett.* **2010,** *10,* 1960–1969

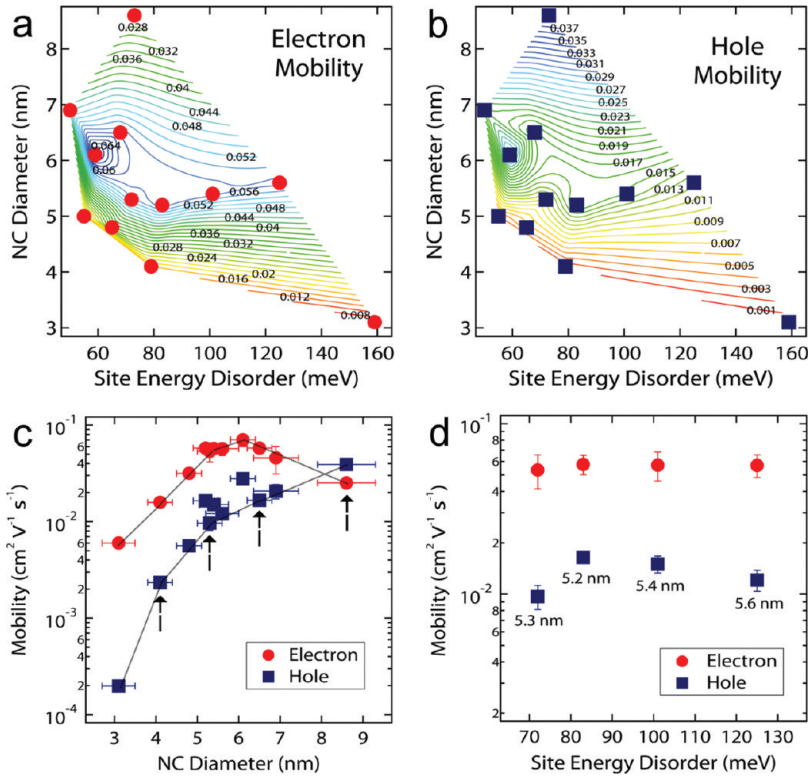

FIGURE 6. Carrier mobility as a function of NC size for ambipolar EDT-treated PbSe NC FETs. Contour plots of (a) electron mobility and (b) hole mobility against NC diameter (*y* axis) and site energy disorder Δα (*x* axis) for devices prepared from 12 different batches of NCs (red and blue markers). (c) The dependence of mobility on NC size. Arrows denote four NC samples of nearly equal energy disorder (indicated in Table 1), showing that mobility depends on NC size rather than the size distribution. Lines serve as guides to the eye. (d) Mobility plotted against energy disorder for four NC samples of very similar size (marked with *b* in Table 1), emphasizing that mobility is independent of the polydispersity of the samples. Many error bars are smaller than the data markers. Each marker represents the average of 6−12 FETs prepared on different days over the course of several months. Channel dimensions: length = 10 μm; width = 1000 μm; film thickness = 20−35 nm.

TABLE 1. Charging Energy, Site Energy Disorder, and Carrier Mobilities of PbSe NC FETs

diameter (nm)	E_C (meV)	Δα (meV)	μ_e ($cm^2\ V^{-1}\ s^{-1}$)	μ_h ($cm^2\ V^{-1}\ s^{-1}$)
3.1	16	159	0.0060	0.00020
4.1[a]	11	79	0.016	0.0023
4.8	9	65	0.032	0.0056
5.0	9	55	0.014	0.0039
5.2[b]	9	83	0.058	0.016
5.3[a,b]	9	72	0.054	0.010
5.4[b]	9	101	0.057	0.015
5.6[b]	8	125	0.057	0.012
6.1	7	59	0.070	0.028
6.5[a]	6	68	0.056	0.017
6.9	6	50	0.046	0.021
8.6[a]	4	73	0.025	0.039

[a] NC samples of equal Δα but different diameter. [b] NC samples of equal diameter but different Δα.

$$C_M \approx 2\pi\varepsilon_0\left(\frac{\varepsilon_{in}(r)\varepsilon_{out}}{\varepsilon_{in}(r) - \varepsilon_{out}}\right) r \ln\left[\frac{2r + d}{d}\right]$$

with $\varepsilon_{in}(r)$ the dielectric constant of the NCs, $\varepsilon_{out} = 2.6$ the dielectric constant of the alkanedithiolate tunnel barriers,[33] r the average NC radius, and d the edge-to-edge separation between NCs. Using $\varepsilon_{in}(r)$ values for PbSe NCs calculated from a generalized Penn model,[5] we find charging energies of only 16 meV for the 3.1 nm NC films and 4 meV for the 8.6 nm NC films (see Table 1). This small spread in E_C can account for only a 60% increase in mobility with NC size, much less than the observed mobility change of 1−2 orders of magnitude. Furthermore, E_C is substantially less than the thermal energy kT (~26 meV). We conclude that the charging energy is of little importance to room-temperature transport in our NC films.

Surprisingly, the carrier mobilities also depend only weakly, if at all, on the site energy disorder (Δα) of the NC films. PbSe NCs are characterized by size-dependent energy levels, and the finite polydispersity of any colloidal NC sample results in a distribution of site energies within a NC film (energy disorder). Charge transport *should* be inhibited by energetic disorder if Δα is of order kT or larger because hopping over long distances then requires thermal assistance (eq 2). We estimate Δα as the width of the first exciton peak (the $1S_h-1S_e$ transition) in NC absorption spectra (Figure S1 in Supporting Information) and find values ranging from 50 to 159 meV (Table 1). Despite the large magnitude and spread of these Δα values, there seems to be no correlation between Δα and the carrier mobilities. For example, FETs made from NCs of similar size but different energy disorder have very similar mobilities (Figure 6d), despite the fact that

DOI: 10.1021/nl101284k | *Nano Lett.* **2010,** *10,* 1960–1969

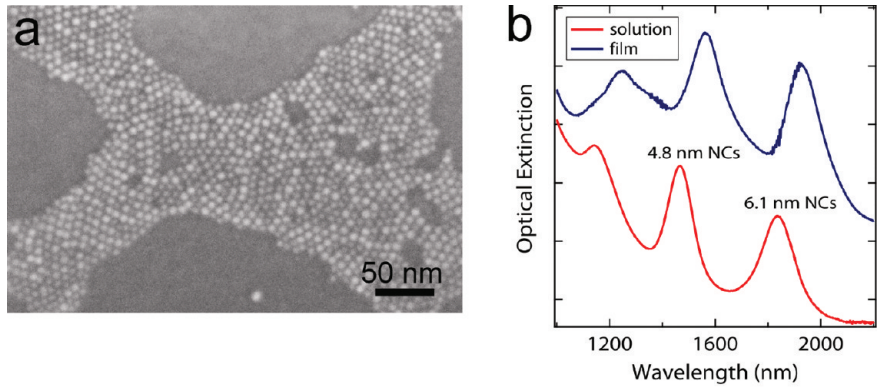

c

FET	μ_e ($cm^2 V^{-1} s^{-1}$)	μ_h ($cm^2 V^{-1} s^{-1}$)
4.8/6.1 mixture	0.011	0.0088
6.1 nm	0.014	0.017
4.8 nm	0.0077	0.0027

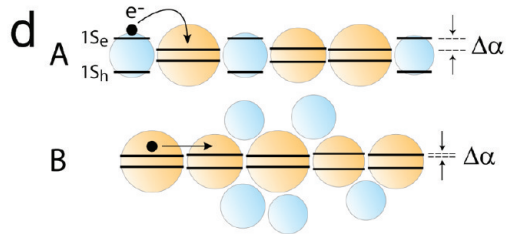

FIGURE 7. FETs made from NCs of two sizes. (a) SEM image of a partial mixed monolayer of 4.8 and 6.1 nm PbSe NCs in the channel of a FET after half of a dip coating cycle (i.e., prior to EDT treatment). Domains and filaments of both small and large NCs are visible. Ten complete dip coating cycles were used to finish these FETs. An image of a complete multilayer film is omitted because the two NC sizes were poorly resolved. (b) Absorption spectra of a mixed film and the parent mixed solution. Such spectra are used to check for "stoichiometric" transfer of NCs from a solution to a film. Spectra are offset for clarity. (c) Carrier mobilities of the pure 4.8 nm, pure 6.1 nm, and mixed NC films. Mobilities for the mixed films are higher than those for the pure 4.8 nm films but less than a factor of 2 smaller than the pure 6.1 nm films. Considering the large difference in site energy between the two NC sizes (~175 meV), the mobilities in a randomly mixed film would be expected to be ~100 times lower than those for either of the pure films. Note that the mobilities of the pure NC films are lower here than in Table 1 because the NC solutions were not freshly prepared for this study. (d) Cartoons of charge transport in the NC films. Transport that involves the entire NC size distribution (path A in a mixed film) results in a relatively large Δα and low mobility, while transport via percolation networks of the larger NCs (path B) has a small Δα and high mobility that is insensitive to the overall polydispersity of the film.

the ratio of Boltzmann factors predicts an 8-fold mobility variation for this series of NC films at room temperature ($\Delta\alpha$ = 72−125 meV). We also made NC FETs with very large energy disorder (200−300 meV) by dip coating from solutions containing equal-weight mixtures of two NC sizes. While such large polydispersities should result in 50−1000 fold lower carrier mobilities for the mixed films, the observed effect is minimal. For instance, FETs composed of mixtures of 4.8 and 6.1 nm NCs have mobilities within a factor of 2 of films of pure 6.1 nm NCs (Figure 7). The insensitivity of mobility to energetic disorder, both in the mixed films and between pure films of different $\Delta\alpha$, suggests that 3D PbSe NC films are heterogeneous on the nanoscale such that carriers injected from the contacts can percolate through continuous networks of the larger diameter, smaller band gap NCs and thereby avoid hops with large activation energies (i.e., those hops from large NCs to small NCs; see Figure 7d). In this picture, mobilities are insensitive to the overall polydispersity of the NC solid as long as continuous percolation pathways exist through some subset of the larger NCs in any given film. Below the percolation threshold, one would expect mobilities to fall precipitously because isolated domains of the larger NCs will act as carrier traps and the full polydispersity of the film will become important to long-range charge transport. Experiments designed to test these ideas in detail are ongoing and will be reported elsewhere.

Having ruled out the charging energy and the site energy disorder as major considerations, we conclude that the increase in mobility with NC size (Figure 6) can be explained by one of two factors, namely (i) the number of carrier hops per unit length of NC film and (ii) the depth of trap states within the NC band gap. Carriers require fewer hops to move a given distance through films of larger NCs. The probability that a carrier moves a macroscopic distance by hopping along a specific pathway is proportional to the product of the tunneling probabilities for that pathway, and the total transport probability is then the sum over all possible pathways. It is thus reasonable for the mobility to increase with NC size because fewer inter-NC hops are needed to

DOI: 10.1021/nl101284k | *Nano Lett.* **2010,** *10,* 1960–1969

transit the FET channel. A second possible explanation for the mobility increase is that larger NCs have shallower trap states. This could occur if the traps (originating from surface defects and adsorbates) are relatively fixed in energy. The band gaps of our NC films vary by more than 600 meV, and a decrease in trap depth of ~100 meV would be enough to account for the observed increase in hole mobility. Studies testing the relative importance of these two factors are underway.

While surely important, the above arguments do not explain other interesting features of Figure 6c, particularly the decrease in electron mobility for large NCs, the larger change in hole mobility, and the quantitative differences between electron and hole mobilities for all NC sizes. We suspect that differences in the energy and concentration of surface states, as well as changes in carrier confinement and carrier density with NC size, play a role here. Simulations of carrier diffusion in 3D NC arrays will be helpful in teasing apart these factors to obtain a quantitative understanding of charge transport in PbX NC solids.

Conclusions. The principal findings of this study are summarized as follows: (i) Alkanedithiol-treated, glassy PbSe NC solids are ambipolar conductors with dark (field-effect) electron mobilities as high as 0.07 $cm^2\ V^{-1}\ s^{-1}$ and hole mobilities 2−6 times lower. Accurate mobility measurements of PbSe NC FETs require fast I_D-V_{SD} and I_D-V_G sweeps. (ii) Carrier mobilities decrease exponentially with increasing ligand length, with a decay length characteristic of hopping transport in granular conductors with alkane tunnel barriers. The mobility of both carrier types increases by a factor of ~2.6 per Å decrease in ligand length. (iii) Mobilities are remarkably insensitive to polydispersity in NC size because conduction seems to be dominated by percolation networks involving only the larger NCs in a film. Severing these low-energy percolation pathways should result in higher average activation energies, pools of trapped charge, and much lower mobilities; (iv) Although insensitive to the size distribution, carrier mobilities increase rapidly with the NC size itself, perhaps because fewer hops are required to move across films composed of larger NCs. However, 3D drift-diffusion simulations of charge transport in NC solids are necessary in order to determine the impact of this and other factors—such as differences in defect states that either facilitate hopping or impede transport by trapping carriers—on the observed size-mobility trends, especially the quantitative differences between the electron and hole mobility and the decrease in electron mobility for the largest NCs.

Our results show that the mobility of carriers in glassy PbSe NC films is determined mostly by the NC size and the coupling energy, the latter of which depends mainly on the size of the inter-NC tunnel barriers. Although the mobility is insensitive to differences in energetic disorder between our NC films, we note that much higher mobilities are possible if energetic and positional disorder could be eliminated so that minibands form between NCs. Achieving long-range coherent transport in NC solids will require high-quality superlattices of monodisperse NCs instead of the glassy NC films studied here. Tuning the tunneling barrier height and improving the superlattice order are important future goals in the creation of high-performance NC solids for optoelectronic applications.

Acknowledgment. We thank Philip Collins, Matthew Beard, and Ara Apkarian for helpful discussions and the UCI Physical Sciences Center for Solar Energy for supporting this work. The authors acknowledge the provision of instrumentation in the Carl Zeiss Center of Excellence at UCI by Carl Zeiss SMT. M.L. is supported by the Center for Advanced Solar Photophysics, an Energy Frontier Research Center funded by the U.S. Department of Energy (DOE), Office of Science, Office of Basic Energy Sciences (BES).

Supporting Information Available. Additional figures showing optical absorption spectra of PbSe NC samples, diameter-band gap relationships, a representative 2D GISAXS pattern for a BuDT-treated film, FTIR spectra of NC films, an AFM image of the 2D film, and UV−vis−NIR absorption measurements. This material is available free of charge via the Internet at http://pubs.acs.org.

REFERENCES AND NOTES

(1) Yu, D.; Wang, C.; Guyot-Sionnest, P. *Science* **2003**, *300*, 1277–1280.
(2) Talapin, D. V.; Murray, C. B. *Science* **2005**, *310*, 86–89.
(3) Konstantatos, G.; Howard, I.; Fischer, A.; Hoogland, S.; Clifford, J.; Klem, E.; Levina, L.; Sargent, E. H. *Nature* **2006**, *442*, 180–183.
(4) Nozik, A. J. *Physica E* **2002**, *14*, 115–120.
(5) Luther, J. M.; Law, M.; Song, Q.; Reese, M. O.; Beard, M. C.; Ellingson, R. J.; Nozik, A. J. *Nano Lett.* **2008**, *8*, 3488–3492.
(6) Koleilat, G. I.; Levina, L.; Shukla, H.; Myrskog, S. H.; Hinds, S.; Pattantyus-Abraham, A.; Sargent, E. H. *ACS Nano* **2008**, *2*, 833–840.
(7) Choi, J. J.; Lim, Y.-F.; Santiago-Berrios, M. B.; Oh, M.; Hyun, B. R.; Sun, L.; Bartnik, A. C.; Goedhart, A.; Malliaras, G. G.; Abruña, H. D.; Wise, F. W.; Hanrath, T. *Nano Lett.* **2009**, *9*, 3749–3755.
(8) Markovich, G.; Collier, C. P.; Henrichs, S. E.; Remacle, F.; Levine, R. D.; Heath, J. R. *Acc. Chem. Res.* **1999**, *32*, 415–423.
(9) Remacle, F. *J. Phys. Chem. A* **2000**, *104*, 4739–4747.
(10) Vanmaekelbergh, D.; Liljeroth, P. *Chem. Soc. Rev.* **2005**, *34*, 299–312.
(11) Luther, J. M.; Law, M.; Song, Q.; Beard, M. C.; Nozik, A. J. *ACS Nano* **2008**, *2*, 271–280.
(12) Law, M.; Beard, M. C.; Choi, S.; Luther, J. M.; Hanna, M. C.; Nozik, A. J. *Nano Lett.* **2008**, *8*, 3904–3910.
(13) Law, M.; Luther, J. M.; Song, Q.; Hughes, B. K.; Perkins, C. L.; Nozik, A. J. *J. Am. Chem. Soc.* **2008**, *130*, 5974–5985.
(14) Kang, M. S.; Lee, J.; Norris, D. J.; Frisbie, C. D. *Nano Lett.* **2009**, *9*, 3848–3852.
(15) Liljeroth, P.; Overgaag, K.; Urbieta, A.; Grandidier, B.; Hickey, S. G.; Vanmaekelbergh, D. *Phys. Rev. Lett.* **2006**, *97*, No. 096803.
(16) Miller, A.; Abrahams, E. *Phys. Rev.* **1960**, *120*, 745–755.
(17) Shklovskii, B. I.; Efros, E. A. *Electronic Properties of Doped Semiconductors*; Springer: Heidelberg, 1984; Chapter 6.
(18) Wold, D. J.; Haag, R.; Rampi, M. A.; Frisbie, C. D. *J. Phys. Chem. B* **2002**, *106*, 2813–2816.
(19) Beebe, J. M.; Engelkes, V. B.; Miller, L. L.; Frisbie, C. D. *J. Am. Chem. Soc.* **2002**, *124*, 11268–11269.
(20) Engelkes, V. B.; Beebe, J. M.; Frisbie, C. D. *J. Am. Chem. Soc.* **2004**, *126*, 14287–14296.

DOI: 10.1021/nl101284k | *Nano Lett.* **2010,** *10,* 1960–1969

(21) Malen, J. A.; Doak, P.; Baheti, K.; Tilley, T. D.; Segalman, R. A.; Majumdar, A. *Nano Lett.* **2009**, *9*, 1164–1169.
(22) Akkerman, H. B.; Naber, R. C. G.; Jongbloed, B.; val Hal, P. A.; Blom, P. W. M.; de Leeuw, D. M.; de Boer, B. *Proc. Natl. Acad. Sci. U.S.A.* **2007**, *104*, 11161–11166.
(23) Wang, W.; Lee, T.; Reed, M. A. *J. Phys. Chem. B* **2004**, *108*, 18398–18407.
(24) Wuelfing, W. P.; Green, S. J.; Pietron, J. J.; Cliffel, D. E.; Murray, R. W. *J. Am. Chem. Soc.* **2000**, *122*, 11465–11472.
(25) Remacle, F.; Beverly, K. C.; Heath, J. R.; Levine, R. D. *J. Phys. Chem. B* **2003**, *107*, 13892–13901.
(26) Tomfohr, J. K.; Sankey, O. F. *Phys. Rev. B* **2002**, *65*, 245105.
(27) Xue, Y.; Datta, S.; Ratner, M. A. *J. Chem. Phys.* **2001**, *115*, 4292–4299.
(28) Koole, R.; Luigjes, B.; Tachiya, M.; Pool, R.; Vlugt, T. J. H.; Donega, C. D. M.; Meijerink, A.; Vanmaekelbergh, D. *J. Phys. Chem. C* **2007**, *111*, 11208–11215.
(29) Kovalenko, M. V.; Scheele, M.; Talapin, D. V. *Science* **2009**, *324*, 1417–1420.
(30) Williams, K. J.; Tisdale, W. A.; Leschkies, K. S.; Haugstad, G.; Norris, D. J.; Aydil, E. S.; Zhu, X.-Y. *ACS Nano* **2009**, *3*, 1532–1538.
(31) Quinn, A. J.; Beecher, P.; Iacopino, D.; Floyd, L.; De Marzi, G.; Shevchenko, E. V.; Weller, H.; Redmond, G. *Small* **2005**, *1*, 613–618.
(32) Lannoo, M.; Delerue, C.; Allan, G. *Phys. Rev. Lett.* **1995**, *74*, 3415–3418.
(33) Porter, M. D.; Bright, T. B.; Allara, D. L.; Chidsey, C. E. D. *J. Am. Chem. Soc.* **1987**, *109*, 3559–3568.

DOI: 10.1021/nl101284k | *Nano Lett.* **2010,** *10,* 1960–1969